Optics & Laser Technology 141 (2021) 107142

Contents lists available at ScienceDirect

Optics and Laser Technology

journal homepage: www.elsevier.com/locate/optlastec

Full length article

A novel processing method based on the 3-spot diode laser source for the laser cladding of stainless-steel ball valves

Xingchen Lin [a,b], Pengfei Wang [a], Hongbo Zhu [b,*], Ziqi Song [c], Yawei Zhang [b], Yongqiang Ning [b]

[a] Science College, Harbin Engineering University, No. 145, Nantong Road, Harbin 150001, China
[b] State Key Laboratory of Luminescence and Applications, Changchun Institute of Optics, Fine Mechanics and Physics, Chinese Academy of Sciences, Changchun 130033, China
[c] Optoelectronic Engineering Department, Aerospace Information Research Institute, Chinese Academy of Sciences, No. 9, Dengzhuang South Road, Beijing 100094, China

ARTICLE INFO

Keywords:
Laser cladding
Diode laser
Stainless-steel material
Microhardness
Ball valve

ABSTRACT

In this paper, aiming to solve the problem of cracks in the laser cladding for stainless-steel ball valves, a novel method for defect-free processing is introduced. To realize this method, a 3-spot high-power diode laser source is developed. These three spots are respectively used for dynamic local preheating, laser cladding processing and dynamic local tempering. Using this high-power diode laser, a cladding processing of the stainless-steel ball valve with Ni60 + WC powder is successfully completed. Compared with the traditional processing approach, the cladded sample is free from any defects such as cracks and pores, which demonstrates the processing effect of this approach. This work provides a new method for the laser cladding of stainless-steel ball valves.

1. Introduction

Laser cladding as an advanced technology for surface treatment can melt the cladding material and the surface of the metallic substrate to form a coating which dramatically improves the corrosion resistance and the wear resistance of the metallic substrate [1,2]. Compared with the traditional arc welding, the laser cladding has distinct advantages, such as controllable input energy, negligible distortion, low dilution and automation process. Despite the high cost of laser sources, the laser cladding has been successfully employed in many industrial fields to repair metallic parts subjected to severe operating conditions.

Among the so many types of laser sources [3,4], due to the high electro-optical efficiency, compactness [5], high metallic absorption and high reliability, high power diode laser source (HPDLS) has become a popular heat source for the laser processing of engineering and manufacturing [6]. Furthermore, HPDLS has a natural rectangular spot which makes it favorable for laser cladding. Many research groups and companies have focused on the technology of the diode laser cladding [7–9]. Y Ding et al. used a 2 kW HPDLS to clad stellite alloy mixture on the seat surface of a control valve, aiming at enhancing the hardness and the wear resistance [10]. Z Weng et al. employed a 3 kW HPDLS to clad Fe-base self-fluxing alloy powder, in order to repair V-grooves on the ductile cast iron substrates [11].

In the petrochemical industry, stainless-steel ball valves are usually used as critical components which are subjected to aggressive operating conditions such as high-pressure steam, mechanical wear and chemical corrosion. In such conditions, the pitting and spalling easily occur on the surface of ball valves after they operating for a period of time, which leads to the leak of the petrochemical material. The reason for this phenomenon is mainly because stainless-steel ball valves have insufficient hardness and low wear resistance. To meet the requirement of above applications, the hardness of ball valves should be at least 550 $HV_{0.1}$, however, the hardness of the stainless-steel material (304) is only approximate 220 $HV_{0.1}$. In order to increase the operating lifetime of stainless-steel ball valves, the laser cladding is necessary to enhance its surface properties like hardness and wear resistance. Unlike other cases, the laser cladding of stainless-steel ball valves is very challengeable. Since the ball valve is a spherical structure, the thermal stress produced by the contraction of substrate volume during its cooling period can lead to the generation of cracks on the substrate surface, which reduces the leakproofness of the ball valve. Thus, how to eliminate cracks of the cladding coating on the ball valves is a key technical problem to be solved, and many efforts have been put forward to this aspect [12,13]. C Lin et al. use the method of the surface preheating to sublimate graphite nodules on the surface of gas turbine casings, in order to enhance the weldability of the substrate and avoid the generation of cracks [14]. S

* Corresponding author.
E-mail address: zhbciomp@163.com (H. Zhu).

https://doi.org/10.1016/j.optlastec.2021.107142
Received 19 March 2020; Received in revised form 14 March 2021; Accepted 7 April 2021
Available online 26 April 2021

Chang et al. also adopt the surface preheating to heat the substrate to 250℃ to prevent cracks in the cobalt-based alloy coating on the seat face of control valves [15]. However, the elimination of cracks in the cladding coating of stainless-steel ball valves has yet be reported so far to our knowledge.

Therefore, aiming to solve this issue, a novel method for the laser cladding of stainless-steel ball valves based on HPDLS is proposed and demonstrated in this paper. Compared with traditional cladding method with prior preheating, this method employing a 3-spot HPDLS can clad stainless-steel ball valves with preheating and tempering in one-time processing, which realizes the defect-free cladding of stainless-steel ball valves. This paper is structured as follows. Firstly, according to this processing method, the development of 3-spot HPDLS is introduced. Three beam spots are respectively used for dynamic local preheating (DLP), laser cladding processing (LCP) and dynamic local tempering (DLT). Secondly, a set of comparative experiments of the laser cladding on the stainless-steel ball valves are carried out. Finally, properties of cladded samples are measured, and a defect-free cladding coating of the stainless-steel ball valve is obtained. This work gives an experimental guide on the laser cladding of stainless-steel ball valves.

2. Development of 3-spot HPDLS

2.1. Beam combination

The diode laser unit employed in this HPDLS is the diode laser stack which is widely used in the development of HPDLS [16,17]. Stacks composed by numerous diode laser bars can easily output several kilowatts power. To further increase the output power, a model based on the beam combination is built, in which two 915 nm stacks and two 976 nm stacks are combined. These stacks have the same structure, and parameters are listed in Table 1. Because the divergence angle of diode laser bars is approximate 70° × 9° (95% power content), every bar should be firstly collimated in the fast axis (FA) by an aspheric cylindrical lens. Then, a group of double cylindrical lenses with a focal length of 200 mm is designed and inserted in the beam path for the slow-axis (SA) collimation. After collimation, the divergence angle of bars is dramatically decreased to 7 mrad × 54 mrad (95% power content).

At present in many ways for increasing output power of HPDLS, beam combination has been demonstrated to an efficient method, because it can scale the power while maintaining a constant beam quality [18,19]. In our case, technologies of polarization beam combination (PBC) and wavelength beam combination (WBC) are implemented. Firstly, in order to make the polarization states of a group of stacks with the same wavelength orthogonal, a half-waveplate is inserted in the collimated beam of one stack. Then, two orthogonally polarized beams are multiplexed together when they reach the polarization beam splitter (PBS). Subsequently, WBC is employed to multiplex two polarization-combined beams with different wavelengths by a dielectric mirror which is typically designed for WBC with a high combining efficiency. Fig. 1 is the structural diagram of the whole beam combination system. After combination, an output power of 6100 W is measured at the injection current of 70 A. Compared with the total initial output power of stacks, there are some losses in the procedures of beam collimation and beam combination.

Table 1
Parameters of diode laser stacks.*

Parameter	Value
Number of stacks	20
Chip width	10 mm
Cavity length	2 mm
Number of emitters	49
Emission width	100 μm
Emitter pitch	200 μm
Filling factor	50%
Pitch of bars	1.9 mm
Θ_{FA}	70°
Θ_{SA}	9°
Output power	1600 W

* Parameters are supplied from product specifications.

2.2. Optical design of 3-spot output

In this work, we propose to adopt a 3-spot HPDLS for cladding the surface of stainless-steel ball valves, thus, an optical system is designed for splitting the combined beam. The schematic diagram is shown in Fig. 2.

In this system, two prisms made of fused silica are inserted in the beam path to refract the upper and lower parts of the combined beam. These two parts of beams deviate from the original path. However, the middle part of the combined beam directly emits along the original path. The far field of three beamlets are shown in Fig. 3.

From Fig. 3 we can see that there are many filamentous beams in each beamlet. The reason for this phenomenon is that diode laser bars in the stacks have small pointing errors, which makes these beams unable to overlap in the far field exactly. After splitting, a pair of field lenses with a focal length of 350 mm is subsequently employed to make these three beamlets convergent and finally focus them to three focal spots on the focal plane. Because diode laser stacks have natural rectangular beams, three focal spots are linear with a top-hat distribution. The corresponding size of three focal spots is 12 mm × 1.5 mm. The space of focal spots (h) is mainly regulated by the angle of prisms, which is calculated by

$$h = f \cdot tan[arcsin(nsin\theta) - \theta], \quad (1)$$

where n and θ respectively denotes the refractive index and the wedge angel of prisms. Furthermore, the power of each part can be controlled by a reasonable position adjustment of prisms, which will not affect the space of focal spots. Considering the previous experience of the laser cladding, the power of three focal spots are respectively set to 1 kW (DLP), 3 kW (LCP) and 2 kW (DLT), and the space of focal spots is 30 mm.

3. Laser cladding experiment

The principle of the laser cladding based on the 3-spot HPDLS is diagrammatically illustrated in Fig. 4. The first beam is used for DLP, which aims to increase the local temperature of the substrate surface, further reducing the temperature gradient. Cladding powder is fed on the substrate surface and after the first focal spot by a powder feeding nozzle. The second beam is used as a main heat source to generate a molten pool on the substrate surface. With the rotation of the ball valve, the cladding powder is delivered into the molten pool, and then rapidly melted and solidified. This relative constant movement between the laser spot and the ball valve makes it possible to generate a cladding coating with a constant thickness. Thermal stress usually occurred in the

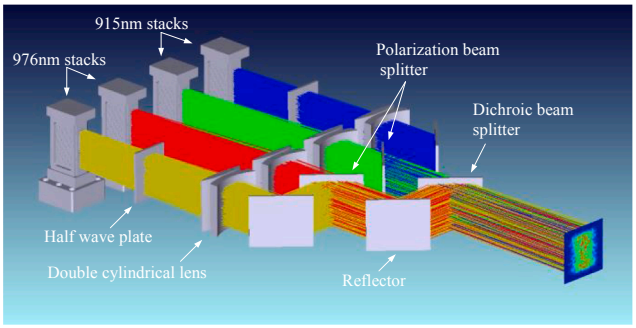

Fig. 1. Structural diagram of beam combination system.

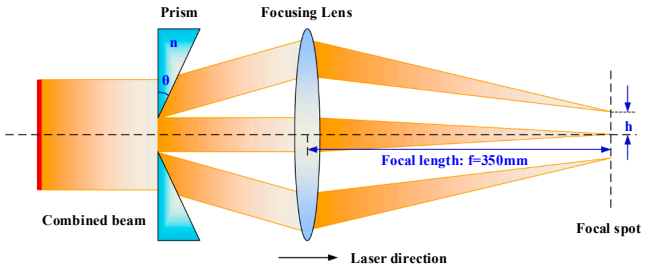

Fig. 2. Schematic diagram of beam splitting optical system for combined beam, n means the reflective index of prisms.

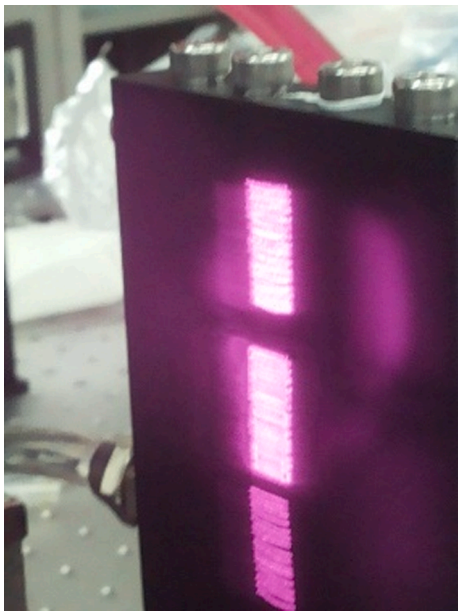

Fig. 3. The far field of three beamlets.

period of the rapid solidification can induce cracks in the laser coating. In this case, the third beam utilized for DLT slows down the cooling rate, which is promising to release residual thermal stress and avoid the generation of cracks.

To demonstrate this novel method for the laser cladding of stainless-steel ball valves, tests are performed using this 3-spot HPDLS. HPDLS is integrated into an industrial machine and fixed over the ball valve. A CNC table is employed to rotate the ball valve with regard to HPDLS. Because the smaller the ball valve is, the bigger the contractility will be, correspondingly causing more difficulty to eliminate cracks. To better verify the cladding effect, the ball valve with a small diameter of 80 mm is adopted in this experiment. The surface of the ball valve is placed on the focal plane of HPDLS. The material of the ball valve is stainless steel 304. The hardness of the ball valve is approximate 220 $HV_{0.1}$.

Usually, Ni-based alloy powder added with hard ceramic particles tungsten carbide (WC) is extensively used as a cladding material to improve the corrosion resistance and the wear resistance. The cladding powder used in the experiment is Ni60 + WC (Wt. ratio: 100:30). The chemical composition of Ni60 + WC powder is shown in Table 2. The size of Ni60 powder particles is in the range of 80 μm–100 μm and that of WC powder particles (angular shape) is in the range of 45 μm–100 μm.

During the laser cladding processing, the cladding powder is usually injected into the processing area through an off-axial or co-axial powder feeding nozzle. However, the laser beam attenuated by the cladding powder can cause the fluctuation of the laser energy, further changing the shape of the molten pool, which has a significant impact on the result of the cladding. To avoid this phenomenon, the method of pre-placed powder feeding is employed in this experiment. Processing parameters of the laser cladding is listed in Table 3. An off-axial feeding nozzle is kept at an angle of 45° to the horizontal. The rectangular exit of the feeding nozzle with a dimension of 10 mm × 2 mm can match the shape of the focal spot. High purity nitrogen gas with a flow rate of 15 L/min is applied as a shielding gas to shield the molten pool from oxidation. To compare the processing effect of this method with the traditional processing method, a group of tests are carried out. In the first test, the second beam of HPDLS with the output of 3 kW is only employed to realize the traditional laser cladding. While in the second test, three beams are all used to process the ball valve. An overlap ratio of 50% is adopted for the multi-track laser cladding in the two tests, which can

Table 2
Chemical composition of Ni60 powder.

	Chemical composition(%)						Fineness
	C	Cr	Si	Fe	Ni	B	
Ni60	0.78	15.9	4.55	5.0max	Bal	/	150/300#
WC	Purity > 99%						140/300#

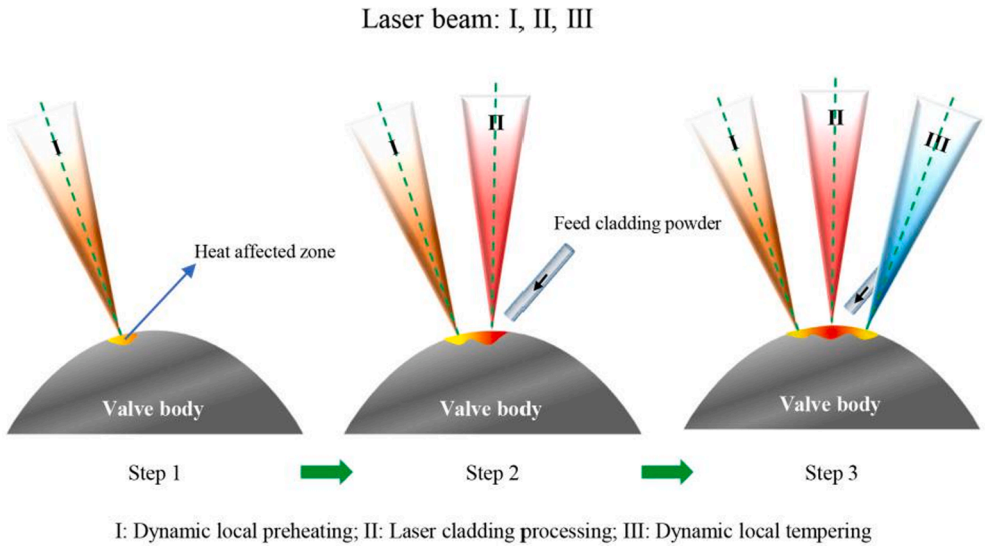

Fig. 4. Schematic diagram of laser cladding based on the 3-spot HPDLS.

Table 3
Processing parameters of the laser cladding.

Parameter	Beam I	Beam II	Beam III
Power	1 kW	3 kW	2 kW
Wavelength	9xx nm		
Scanning speed	300 mm/min		
Dimension of feeding nozzle	10 mm × 2 mm		
Angle of feeding nozzle	45° to the horizontal		
Shielding gas	high purity nitrogen gas		
Flow rate	15 L/min		

produce a uniform cladding thickness about 1.4 mm. After the processing, a liquid dye penetrant test with color indication is used to detect cracks presented in the cladding coating of the ball valve. Cladded samples can be visually inspected by this test, which are shown in Fig. 5.

From Fig. 5(a), we can see that a lot of cracks appear in the cladding coating of the ball valve. This is attributed to that the coefficient of thermal expansion (CTE) of the cladding coating is much different from the substrate. Therefore, the high cooling rate causes the major thermal stress, which can lead to the generation of cracks during the cooling. In Fig. 5(b), however, no visible cracks is found in the cladding coating, which preliminarily proves that the laser cladding based on the 3-spot HPDLS can eliminate cracks effectively.

The average hardness of two cladded samples measured by a Rockwell hardness tester are about HRC58 (cladded in the traditional processing method) and HRC54 (cladded by the 3-spot HPDLS), respectively. Though the third beam used for DLT causes "back tempering" for the previous cladded area, comparing with the original hardness, the hardness of the sample cladded by 3-spot HPDLS is drastically increased, which can meet the requirement of most industrial applications.

Specimens for the microstructural analysis are cut from the 3-spot cladded ball valve using a wire-electrode cutting machine. Fig. 6(a) shows the cross-sectional micrographs of the cladding coating. The grey phase in the coating mainly consists of WC particles. It is worthwhile

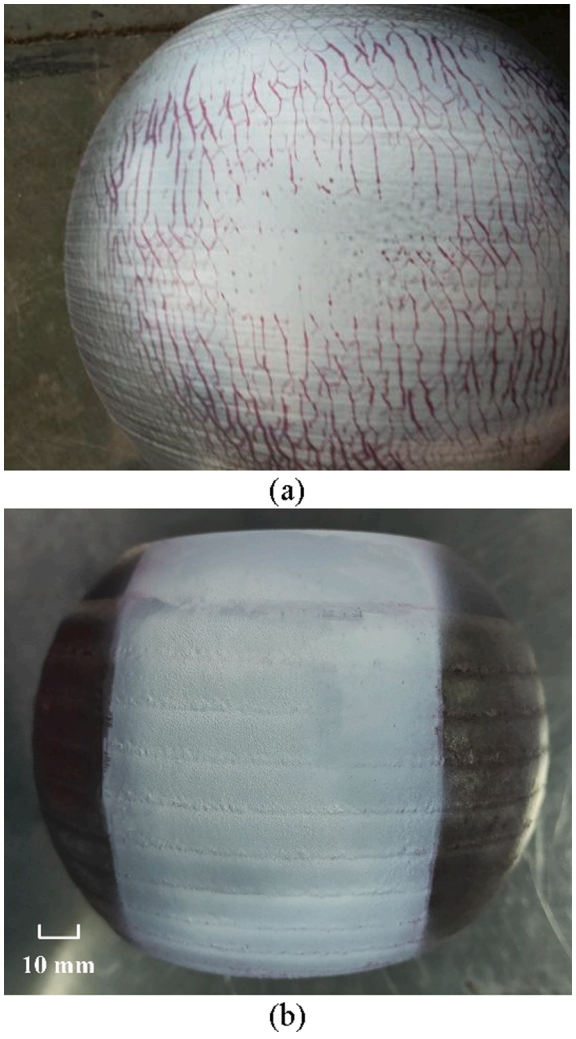

Fig. 5. Liquid dye penetrant test with color indication for cracks inspection. (a) Traditional processing method with single laser beam (b) Laser cladding based on the 3-spot HPDLS.

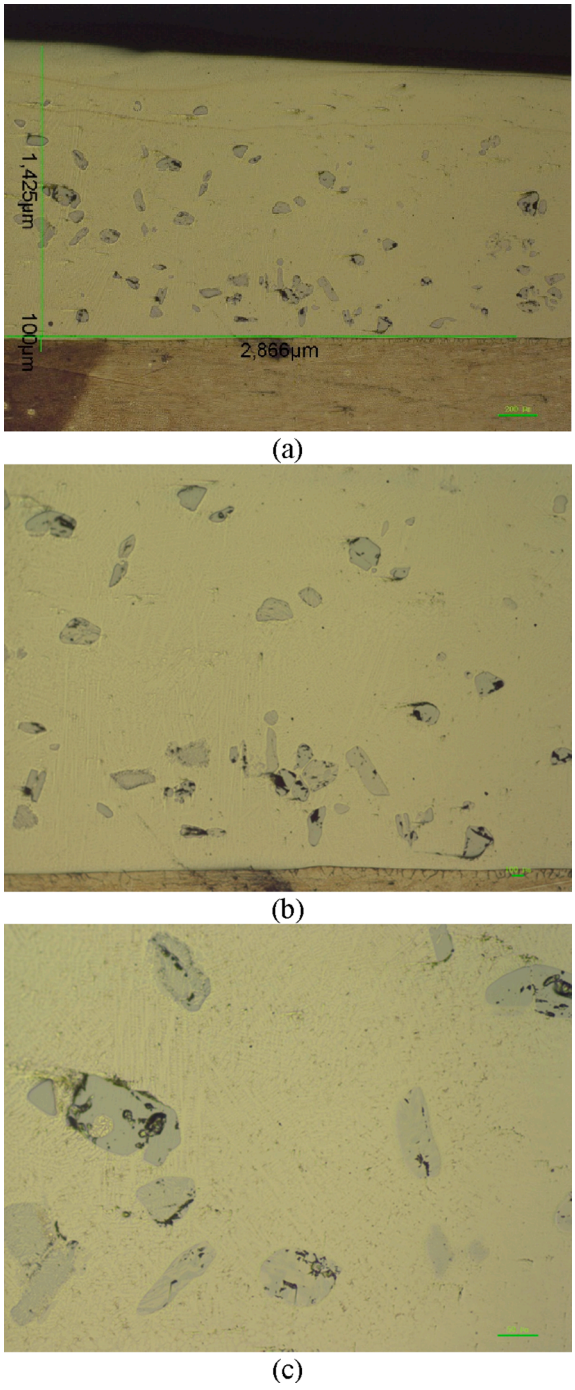

Fig. 6. Cross-sectional micrographs of the cladded specimen under the various magnifications (a) 50× magnification, the green scale shows a cladding coating height of 1.4 mm, (b) 100× magnification, (c) 200× magnification.

noting that the distribution of WC particles is not uniform throughout the coating. WC particles are mainly placed at the lower position of the coating, which can be attributed to that the lower melting point and slower solidification rate of the Ni60 matrix make WC particles tend to sink when the Ni60 matrix solidifies. Micrographs (b) and (c) are used to further inspect pores and microcracks, from which we can found no defects in the cladding coating.

The microhardness across the cross section of the cladded specimen is measured by a Vickers-1000 tester with $HV_{0.1}$ load for 10-s dwell time, and measurement locations are shown in Fig. 7. The distance between measurement locations is 0.05 mm.

The measured average microhardness value of each location is shown in Fig. 8. The cladding layer is denoted by A in the picture. The upper part of the cladding layer (0–0.5 mm) mainly consists of Ni60 matrix, and the average microhardness fluctuates from 590 $HV_{0.1}$ to 630 $HV_{0.1}$. In the lower part of the cladding layer (0.5 mm–1.4 mm), the microhardness increases from 630 $HV_{0.1}$ to 703 $HV_{0.1}$. We already discuss that WC particles sink toward to the lower position of the cladding coating, which makes this layer have the higher hardness. Usually, ball valves after the laser cladding are grinded by the machine to recover the original diameter, so this highest hardness layer is exposed, which can dramatically increase the hardness and wear resistance of the substrate surface. In the bonding zone (1.4 mm–1.6 mm) denoted by B, the average microhardness decreases from 703 $HV_{0.1}$ to 533 $HV_{0.1}$. This variation could be the result of an alloy layer formed by the cladding material and substrate. Under this layer is the heat affected zone (1.6 mm–1.8 mm), marked by C, the average microhardness decreases further from 533 $HV_{0.1}$ to 223 $HV_{0.1}$. This is because that, with the deepening of the processing depth, the substrate is not highly affected by the laser radiation. D region is the substrate which is not affected by the laser radiation, so the microhardness has a steady value of about 220 $HV_{0.1}$.

4. Conclusion

(1) In this paper, in order to eliminate cracks in the laser cladding coating on the stainless-steel ball valves, a novel processing method based on the 3-spot HPDLS has been introduced and demonstrated. In this method, three beam spots are employed for increasing the local temperature of the substrate surface, cladding the coating and slowing down the cooling rate, respectively.
(2) Using this method, when three beam spots are set to 1 kW (DLP), 3 kW (LCP) and 2 kW (DLT), a laser cladding processing of the stainless-steel ball valve is successfully completed with Ni60 + WC powder. Through a liquid dye penetrant test with color indication, we can see that cracks and pores in the cladding coating of the ball valve are effectively eliminated.
(3) The average hardness and the highest microhardness are investigated, and the results are HRC54 and 703 $HV_{0.1}$, respectively, which can meet the most requirements of industrial applications.
(4) In the traditional laser cladding, to eliminate cracks of the cladding coating, cladding samples are usually preheated with an induction heater (coil) before the processing [20–22]. After the processing, cladding samples are tempered at high temperature for several hours in order to relief the stress [23]. This is very complex and time consuming to process a sample. Comparing with the traditional method for eliminating cracks, this method can process the ball valve in one-time, which greatly increase the processing efficiency.
(5) This work not only provides a novel method for laser cladding of the stainless-steel ball valve, but also paves the way for the future research of the diode laser processing.

Declaration of Competing Interest

The authors declare that they have no known competing financial interests or personal relationships that could have appeared to influence the work reported in this paper.

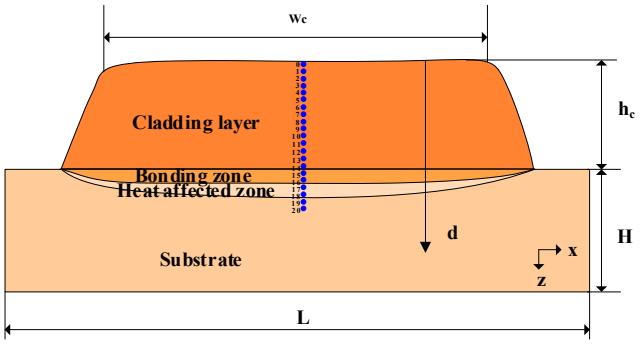

Fig. 7. Measurement locations of microhardness across the cross section. Cross section consists of four regions, cladding layer, bonding zone, heat affect zone and substrate.

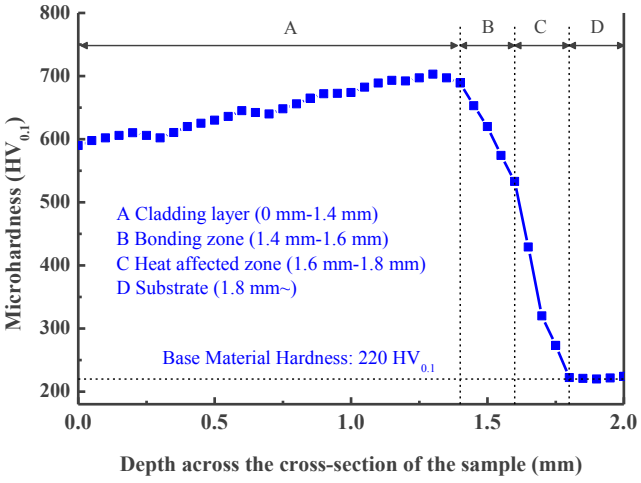

Fig. 8. Measured cross-sectional microhardness distribution.

Acknowledgement

This work was supported by the National Natural Science Foundation of China (NSFC) (61674149).

References

[1] F. Arias-Gonzalez, J.D. Val, R. Comesana, J. Penide, F. Lusquinos, F. Quintero, A. Riverro, M. Boutinguiza, J. Pou, Fiber laser cladding of nickel-based alloy on cast iron, Appl. Surf. Sci. 374 (2016) 197–205.
[2] L. Huaming, Q. Xunpeng, H. Song, H. Zeqi, N. Mao, Geometry modeling of single track cladding deposited by high power diode laser with rectangular beam spot, Opt. Lasers Eng. 100 (2018) 36–46.
[3] S.S. Patrick, J.B. Matin, Adaptive optics in laser processing, Light: Sci. Appl. 8 (2019) 1–16.
[4] B.W. Tilma, M. Mangold, C.A. Zaugg, S.M. Link, D. Waldburger, A. Klenner, A. S. Mayer, E. Gini, M. Golling, U. Keller, Recent advances in ultrafast semiconductor disk lasers, Light: Sci. Appl. 4 (2015) e310.
[5] Y. Sun, K. Zhou, M. Feng, Z. Li, Y. Zhou, Q. Sun, J. Liu, L. Zhang, D. Li, S. Zhang, M. Ikeda, H. Yang, Room-temperature continuous-wave electrically pumped InGaN/GaN quantum well blue laser diode directly grown on Si, Light Sci. Appl. 7 (2018) 13.
[6] Y. Mei, G.E. Weng, B.P. Zhang, J.P. Liu, W. Hofmann, L.Y. Ying, J.Y. Zhang, Z.C. Li, H. Yang, H.C. Kuo, Quantum dot vertical-cacity surface-emitting lasers covering the 'green gap, Light Sci. Appl. 6 (2017) e16199.
[7] J.A. Alcock, B. Baufeld, Diode laser welding of stainless steel 304L, J. Mater. Process. Technol. 240 (2017) 138–144.
[8] H. Zhu, S. Fan, Jian Z, X. Lin, L. Qin, Y. Ning, Development and thermal management of kW-class high-power diode laser source based on the structure of two-stage combination 11 (2019) 1502510.

[9] F. Wang, L. Zhong, X. Tang, C. Xu, C. Wan, A homogeneous focusing system for diode laser and its applications in metal surface modification, Opt. Laser Technol. 102 (2018) 197–206.
[10] D. Yinping, L. Rong, Y. Jianhua, Z. Qunli, W. Liang, Stellite alloy mixture hardfacing via laser cladding for control calce seat sealing surfaces, Surf. Coat. Technol. 329 (2017) 97–108.
[11] Z. Weng, A. Wang, X. Wu, Y. Wang, Z. Yang, Wear resistance of diode laser-clad Ni/WC composite coatings at different temperatures, Surf. Coat. Technol. 304 (2016) 283–292.
[12] S. Santhanakrishnan, F. Kong, R. Kovacevic, An experimentally based thermo-kinetic hardening model for high power direct diode laser cladding, J. Mater. Process. Technol. 211 (2011) 1247–1259.
[13] Z. Zhang, P. Farahmand, R. Kadovan, Laser cladding of 420 stainless with molybdenum on mild steel A36 by a high power direct diode laser, Mater. Des. 109 (2016) 686–699.
[14] C.M. Lin, A.S. Chandra, L. Morales-Rivas, S.Y. Huang, H.C. Wu, Y.E. Wu, H.L. Tsai, Repair welding of ductile cast iron by laser cladding process: microstructure and mechanical properties, Int. J. Cast Met. Res. 27 (2013) 378–383.
[15] S.S. Chang, H.C. Wu, C. Chen, Impact wear resistance of stellte 6 hardfaced valve seats with laser cladding, Int. J. Cast Met. Res. 23 (2008) 708–713.
[16] H. Zhu, M. Hao, J. Zhao, W. Ji, X. Lin, J. Zhang, Y. Ning, Development and thermal management of 10 kW CW, direct diode laser source, Opt. Laser Technol. 76 (2016) 101–105.
[17] J. Malchus, V. Krause, A. Koesters, D.G. Matthews, A 25kW fiber-coupled diode laser for pumping applications, Proc. of SPIE 8965 (2014) 89650B.
[18] H. Zhu, X. Lin, Y. Zhang, J. Zhang, B. Wang, J. Zhang, L. Qin, Y. Ning, H. Wu, kW-class fiber-coupled diode laser source based on dense spectral multiplexing of an ultra-narrow channel spacing, Opt. Express 26 (2018) 24723–24733.
[19] U. Witte, F. Schneider, M. Traub, D. Hoffmann, S. Drovs, T. Brand, A. Unger, kW-class direct diode laser for sheet metal cutting based on DWDM of pump modules by use of ultra-steeo dielectric filters, Opt. Express 24 (2016) 22917–22929.
[20] C.M. Lin, A.S. Chandra, L. Morales Rivas, S.Y. Huang, H.C. Wu, Y.E. Wu, H.L. Tsai, Repair welding of ductile cast iron by laser cladding process: microstructure and mechanical properties, Int. J. Cast Met. Res. 27 (2014) 378–383.
[21] P. Yi, P. Xu, C. Fan, C.I. Li, Y. Shi, The effect of dynamic local self-preheating in laser cladding on grey cast iron, J. Mech. Eng. 61 (2015) 43–52.
[22] J.S. Xu, X.C. Zhang, F.Z. Xuan, F.Q. Tian, Z.D. Wang, S.T. Tu, Tensile properties and fracture behavior of laser cladded WC/Ni composite coatings with different contents of WC particle studied by in-situ tensile testing, Mater. Sci. Eng., A 560 (2013) 744–751.
[23] S.S. Chang, H.C. Wu, C. Chen, Impact wear resistance of stellite 6 hardfaced valve seats with laser cladding, Mater. Manuf. Processes 23 (2008) 708–713.